
VARIATIONAL PHYSICS INFORMED NEURAL NETWORKS: THE ROLE OF QUADRATURES AND TEST FUNCTIONS

A PREPRINT

Stefano Berrone*

Claudio Canuto*

Moreno Pintore*

September 7, 2021

ABSTRACT

In this work we analyze how Gaussian or Newton-Cotes quadrature rules of different precisions and piecewise polynomial test functions of different degrees affect the convergence rate of Variational Physics Informed Neural Networks (VPINN) with respect to mesh refinement, while solving elliptic boundary-value problems. Using a Petrov-Galerkin framework relying on an inf-sup condition, we derive an a priori error estimate in the energy norm between the exact solution and a suitable high-order piecewise interpolant of a computed neural network. Numerical experiments confirm the theoretical predictions, and also indicate that the error decay follows the same behavior when the neural network is not interpolated. Our results suggest, somehow counterintuitively, that for smooth solutions the best strategy to achieve a high decay rate of the error consists in choosing test functions of the lowest polynomial degree, while using quadrature formulas of suitably high precision.

Keywords Variational Physics Informed Neural Networks, quadrature formulas, inf-sup condition, a priori error estimate, convergence rates, elliptic problems

MSC-class 35B45, 35J20, 35Q93, 65K10, 65N20, 68T07

1 Introduction

Exploiting the recent advances in artificial intelligence and, in particular, in deep learning, several innovative numerical techniques have been developed in the last few years to compute numerical solutions of partial differential equations (PDEs). In such methods, the solution is approximated by a neural network that is trained by taking advantage of the knowledge of the underlying differential equation. One of the earliest models involving a neural network was described in [19]: it is based on the concept of Physics Informed Neural Networks (PINN) and it inspired further works such as e.g. [27] or [30], until the recent paper [14] which presents a very general framework for the solution of operator equations by deep neural networks.

In such papers, given an arbitrary PDE coupled with proper boundary conditions, the training of the PINN aims at finding the weights \mathbf{w} of a neural network such that the associated function $u^{\mathcal{N}}(\mathbf{x}; \mathbf{w})$ minimizes some functional of the equation residual while satisfying as much as possible the imposed boundary conditions. To do so, the neural network is trained to minimize the residual only at a finite set of collocation points, and additional terms are added to the loss function in order to force the network to approximately satisfy the boundary conditions. Thanks to the good approximation properties of neural networks, formally proved e.g. in [4], [7], [17], [13], [18] and [6] under suitable assumptions, the PINN approach looks very promising because it is able to efficiently and accurately compute approximated solutions of arbitrary PDEs encoding their structures in the loss function.

Subsequently, the PINN paradigm has been further developed in [10] to obtain the so-called Variational Physics Informed Neural Networks (VPINN). The main differences with respect to the PINN are that the weak formulation of the PDE is exploited, the collocation points are replaced by test functions, and quadrature points are used to compute the integrals involved in the variational residuals. In such methods the solution is still approximated by a neural network, but the test functions are represented by a finite set of known functions or by a second neural network (see [31]); therefore, the technique can be seen as a Petrov-Galerkin method. The method is more flexible than the

*Dipartimento di Scienze Matematiche, Politecnico di Torino, Corso Duca degli Abruzzi 24, 10129 Torino, Italy. stefano.berrone@polito.it (S. Berrone), claudio.canuto@polito.it (C. Canuto), moreno.pintore@polito.it (M. Pintore).

standard PINN because integration by parts, involved in the weak formulation, decreases the required regularity of the approximate solution. Furthermore, the fact that the dataset used in the training phase consists of quadrature points significantly reduces the computational cost of the training phase. Indeed, quadrature points are, in general, much fewer than collocation points.

Combining the VPINN with the Finite Element Method (FEM), the authors of [12] developed VarNet, a VPINN that exploits the test functions of the \mathbb{P}_1 -FEM. Such a work has been then extended in [11] to consider arbitrary high-order polynomials as test functions, as in the hp version of the FEM. Although the authors of the cited works empirically observed that both PINNs and VPINNs are able to efficiently approximate the desired solution, no proof of convergence and estimate of convergence rate is provided for VPINNs. Instead, for PINNs, rigorous a priori error analysis are already available in, for instance, [15].

The purpose of this paper is to investigate how the choice of piecewise polynomial test functions and quadrature formulas influences the accuracy of the resulting VPINN approximation of second-order elliptic problems. One might think that test functions of high polynomial degree are needed to get a high order of accuracy; we prove that this is not the case, actually we indicate that precisely the opposite is true: it is more convenient to keep the degree of test functions as low as possible, while using quadrature formulas of precision as high as possible. Indeed, for sufficiently smooth solutions, the error decay rate is given by

$$q + 2 - k_{test},$$

where q is the precision of the quadrature formula and k_{test} is the degree of the test functions.

Using a Petrov-Galerkin framework, we derive an a priori error estimate in the energy norm between the exact solution and a suitable piecewise polynomial interpolant of the computed neural network; we assume that the architecture of the neural network is fixed and sufficiently rich, and we explore the behavior of the error versus the size of the mesh supporting the test functions. Our analysis relies upon the validity of an inf-sup condition between the spaces of test functions and the space in which the neural network is interpolated.

A variety of numerical experiments confirms the theoretical prediction. Interestingly, in our experiments the error between the exact solution and the computed neural network decays asymptotically with the same rate as predicted by our theory for the interpolant of the network; however, this behavior cannot be rigorously guaranteed, since in general the minimization problem which defines the computed neural network is underdetermined, and the computed neural network may be affected by spurious components. Indeed, we show that for a problem with zero data the minimization of the loss function may yield non-vanishing neural networks. With the method proposed in this paper, we combine the efficiency of the VPINN approach with the availability of a sound and certified convergence analysis.

The paper is organized as follows. In Sect. 2 we introduce the elliptic problem we are focusing on, and we also present the way in which the Dirichlet boundary conditions are exactly imposed, which is uncommon in PINNs and VPINNs but can be generalized as in [26]. In Sect. 3 we focus on the numerical discretization; in particular, the involved NN architecture is described in Sect. 3.1 while the problem discretization and the corresponding loss function are described in Sect. 3.2. Here we also introduce an interpolation operator \mathcal{I}_H applied to the neural networks. Sect. 4 is the key section: through a series of preliminary results, we formally derive the a priori error estimate, the main result being Theorem 4.9. In Sect. 5 we specify the parameters of the neural network used for the numerical tests and the training phase details. We also analyze the consequences of fulfilling the inf-sup condition in connection with the VPINN efficiency. Numerous numerical tests are presented and discussed in Sect. 6 for one-dimensional and two dimensional elliptic problems. Such a collection empirically confirms the validity of the a priori estimate in different scenarios. Finally, in Sect. 7, we draw some conclusion and we highlight the future perspective of the current work.

2 The model boundary-value problem

Let $\Omega \subset \mathbb{R}^n$ be a bounded polygonal/polyhedral domain with boundary $\Gamma = \partial\Omega$, partitioned into $\Gamma = \Gamma_D \cup \Gamma_N$ with $\Gamma_D \cap \Gamma_N = \emptyset$ and $\text{meas}_{n-1}(\Gamma_D) > 0$.

Let us consider the model elliptic boundary-value problem

$$\begin{cases} Lu := -\nabla \cdot (\mu \nabla u) + \beta \cdot \nabla u + \sigma u = f & \text{in } \Omega, \\ u = g & \text{on } \Gamma_D, \\ \mu \frac{\partial u}{\partial n} = \psi & \text{on } \Gamma_N, \end{cases} \quad (2.1)$$

where $\mu, \sigma \in L^\infty(\Omega)$, $\beta \in (W^{1,\infty}(\Omega))^n$ satisfy $\mu \geq \mu_0$, $\sigma - \frac{1}{2} \nabla \cdot \beta \geq 0$ in Ω for some constant $\mu_0 > 0$, whereas $f \in L^2(\Omega)$, $g \in \bar{u}|_{\Gamma_D}$ for some $\bar{u} \in H^1(\Omega)$, and $\psi \in L^2(\Gamma_N)$.

Define the spaces $U = H^1(\Omega)$, $V = H_{0,\Gamma_D}^1(\Omega) := \{v \in U : v|_{\Gamma_D} = 0\}$, the bilinear form $a : U \times V \rightarrow \mathbb{R}$ and the linear form $F : V \rightarrow \mathbb{R}$ such that

$$a(w, v) = \int_{\Omega} \mu \nabla w \cdot \nabla v + \beta \cdot \nabla w v + \sigma w v, \quad F(v) = \int_{\Omega} f v + \int_{\Gamma_N} \psi v; \quad (2.2)$$

denote by $\alpha \geq \mu_0$ the coercivity constant of the form a , and by $\|a\|, \|F\|$ the continuity constants of the forms a and F . Problem (2.1) is formulated variationally as follows: *Find $u \in \bar{u} + V$ such that*

$$a(u, v) = F(v) \quad \forall v \in V. \quad (2.3)$$

We assume that we can represent u in the form

$$u = \bar{u} + \Phi \tilde{u}, \quad (2.4)$$

for some (known) smooth function $\Phi \in V$ and some $\tilde{u} \in U$ having the same smoothness of u . Let us introduce the affine mapping

$$B : U \rightarrow \bar{u} + V \quad \text{such that} \quad Bw = \bar{u} + \Phi w \quad (2.5)$$

which enforces the given Dirichlet boundary condition. Then, Problem (2.3) can be equivalently formulated as follows: *Find $\tilde{u} \in U$ such that*

$$a(B\tilde{u}, v) = F(v) \quad \forall v \in V. \quad (2.6)$$

Remark 2.1 (Enforcement of the Dirichlet conditions). The approach we follow to enforce Dirichlet boundary conditions will allow us to deal with a loss function which is built solely by the residuals of the variational equations. Other approaches are obviously possible: for instance, one could augment such loss function by a term penalizing the distance of the numerical solution from the data on Γ_D , or adopt a Nitsche's type variational formulation of the boundary-value problem [16]. Both strategies involve parameters which may need a tuning, whereas in our approach the definition of the loss function is simple and natural, allowing us to focus on the performances of the neural networks.

3 The VPINN-based numerical discretization

In this section, we first introduce the class of neural networks used in this paper, then we describe the numerical discretization of the boundary-value problem (2.6), which uses neural networks to represent the discrete solution and piecewise polynomial functions to enforce the variational equations. An inf-sup stable Petrov-Galerkin formulation is introduced which guarantees stability and convergence, as indicated in Sect. 4; this is the main difference of the proposed method with respect to other formulations, such as [10, 11].

3.1 Neural networks

In this work we only use fully-connected feed-forward neural networks (named also multi-layered perceptrons), therefore the following description is focused on such a class of networks. Since we deal with a scalar equation, a neural network will be a function $w : \mathbb{R}^n \rightarrow \mathbb{R}$ defined as follows: for any $\mathbf{x} \in \mathbb{R}^n$, the output $w(\mathbf{x})$ is computed via the chain of assignments

$$\begin{aligned} \mathbf{x}_0 &= \mathbf{x}, \\ \mathbf{x}_\ell &= \rho(\mathbf{A}_\ell \mathbf{x}_{\ell-1} + \mathbf{b}_\ell), \quad \ell = 1, \dots, L-1, \\ w(\mathbf{x}) &= \mathbf{A}_L \mathbf{x}_{L-1} + b_L. \end{aligned} \quad (3.1)$$

Here, $\mathbf{A}_\ell \in \mathbb{R}^{N_\ell \times N_{\ell-1}}$ and $\mathbf{b}_\ell \in \mathbb{R}^{N_\ell}$, $\ell = 1, \dots, L$, are matrices and vectors that store the network weights (with $N_0 = n$ and $N_L = 1$); furthermore, L is the number of layers, whereas ρ is the (nonlinear) activation function which acts component-wise (i.e. $\rho(\mathbf{y}) = [\rho(y_1), \dots, \rho(y_{n_y})]$ for any vector $\mathbf{y} \in \mathbb{R}^{n_y}$). It can be noted from equation (3.1), that if $\rho \in C^k(\mathbb{R})$, then w inherits the same regularity because it can be seen as a composition of functions belonging to $C^k(\mathbb{R})$. Popular choices include the ReLU ($k = 0$) and RePU ($k > 0$ finite) functions, as well as the hyperbolic tangent ($k = \infty$) if one wants to exploit the maximum of regularity in the solution of interest.

The neural network structure \mathcal{NN} is identified by fixing the number of layers L , the integers N_ℓ and the activation function ρ . The entire set of weights that parametrize the network can be logically organized into a single vector $\mathbf{w} \in \mathbb{R}^N$. Thus, the neural network structure \mathcal{NN} induces a mapping

$$\mathcal{F}^{\mathcal{NN}} : \mathbb{R}^N \rightarrow C^\infty(\bar{\Omega}), \quad \mathbf{w} \mapsto \mathcal{F}^{\mathcal{NN}}(\mathbf{w}) = w, \quad \text{where } w = w(\mathbf{x}, \mathbf{w}). \quad (3.2)$$

It is convenient to define the manifold

$$U^{\mathcal{NN}} \subset U, \quad U^{\mathcal{NN}} = \mathcal{F}^{\mathcal{NN}}(\mathbb{R}^N)$$

containing all functions that can be generated by the neural network structure \mathcal{NN} .

3.2 The VPINN discretization

We aim at approximating the solution of Problem (2.1) by a generalized Petrov-Galerkin strategy. To this end, let us introduce a conforming, shape-regular triangulation $\mathcal{T}_h = \{E\}$ of $\bar{\Omega}$ with meshsize $h > 0$ and, for a fixed integer $k_{\text{test}} \geq 1$, let $V_h \subset V$ be the linear subspace formed by the functions which are piecewise polynomials of degree k_{test} over the triangulation \mathcal{T}_h . Furthermore, let us introduce computable approximations of the forms a and F by numerical quadratures. Precisely, for any $E \in \mathcal{T}_h$, let $\{(\xi_\iota^E, \omega_\iota^E) : \iota \in I^E\}$ be the nodes and weights of a quadrature formula of precision

$$q \geq 2k_{\text{test}} \quad (3.3)$$

on E . Assume that Γ_N is the union of a collection $\partial\mathcal{T}_h(\Gamma_N)$ of edges of elements of \mathcal{T}_h ; for any such edge e , let $\{(\xi_\iota^e, \omega_\iota^e) : \iota \in I^e\}$ be the nodes and weights of a quadrature formula of precision q on e . Then, assuming that all the data $\mu, \beta, \sigma, f, \psi$ are continuous in each element of the triangulation, we define the approximate forms

$$a_h(w, v) = \sum_{E \in \mathcal{T}_h} \sum_{\iota \in I^E} [\mu \nabla w \cdot \nabla v + \beta \cdot \nabla w v + \sigma w v](\xi_\iota^E) \omega_\iota^E, \quad (3.4)$$

$$F_h(v) = \sum_{E \in \mathcal{T}_h} \sum_{\iota \in I^E} [f v](\xi_\iota^E) \omega_\iota^E + \sum_{e \in \partial\mathcal{T}_h(\Gamma_N)} \sum_{\iota \in I^e} [\psi v](\xi_\iota^e) \omega_\iota^e. \quad (3.5)$$

With these ingredients at hand, we would like to approximate the solution of Problem (2.6) by some $u^{\mathcal{NN}} \in U^{\mathcal{NN}}$ satisfying

$$a_h(Bu^{\mathcal{NN}}, v_h) = F_h(v_h) \quad \forall v_h \in V_h. \quad (3.6)$$

Such a problem might be ill-posed when, for computational efficiency, the dimension of the test space V_h is chosen smaller than the dimension of the manifold $U^{\mathcal{NN}}$. In this situation, we get an under-determined problem, with obvious difficulties in deriving stability estimates on some norms of the function $Bu^{\mathcal{NN}}$. Actually, Problem (3.6) with zero data (i.e., zero f, g, ψ) could admit non-zero solutions (see Section 6.3).

To avoid these difficulties, we adopt the strategy of applying a projection (indeed, an interpolation) to the function $Bu^{\mathcal{NN}}$, mapping it into a finite dimensional space of dimension comparable to that of V_h , and we content ourselves with estimating some norm of this projection.

To be precise, let us introduce a conforming, shape-regular partition $\mathcal{T}_H = \{G\}$ of $\bar{\Omega}$, which is equal to or coarser than \mathcal{T}_h (i.e., each element $E \in \mathcal{T}_h$ is contained in an element $G \in \mathcal{T}_H$) but compatible with \mathcal{T}_h (i.e., its meshsize $H > 0$ satisfies $H \lesssim h$). Let the integer $k_{\text{int}} \geq 1$ be defined by the condition

$$k_{\text{int}} + k_{\text{test}} = q + 2. \quad (3.7)$$

Let $U_H \subset U$ be the linear subspace formed by the functions which are piecewise polynomials of degree k_{int} over the triangulation \mathcal{T}_H , and let $U_{H,0} = U_H \cap V$ be the subspace of U_H formed by the functions vanishing on Γ_D . Finally, let $\mathcal{I}_H : C^0(\bar{\Omega}) \rightarrow U_H$ be an interpolation operator, satisfying the condition $\mathcal{I}_H : C^0(\bar{\Omega}) \cap V \rightarrow U_{H,0}$ as well as the following approximation properties: for all $v \in H^{k+1}(\Omega)$, $1 \leq k \leq k_{\text{int}}$,

$$|v - \mathcal{I}_H v|_{\ell, G} \lesssim H^{k+1-\ell} |v|_{k+1, G}, \quad 0 \leq \ell \leq k+1, \quad \forall G \in \mathcal{T}_H. \quad (3.8)$$

In this framework, assuming the lifting \bar{u} to be continuous in $\bar{\Omega}$, we replace the target equations (3.6) by the following ones:

$$a_h(\mathcal{I}_H Bu^{\mathcal{NN}}, v_h) = F_h(v_h) \quad \forall v_h \in V_h. \quad (3.9)$$

In order to handle this problem by the neural network, let us introduce a basis in V_h , say $V_h = \text{span}\{\varphi_i : i \in I_h\}$, and for any w smooth enough let us define the residuals

$$r_{h,i}(w) = F_h(\varphi_i) - a_h(\mathcal{I}_H Bw, \varphi_i), \quad i \in I_h, \quad (3.10)$$

as well as the loss function

$$R_h^2(w) = \sum_{i \in I_h} r_{h,i}^2(w) \gamma_i^{-1}, \quad (3.11)$$

where $\gamma_i > 0$ are suitable weights. Then, we search for a global minimum of the loss function in $U^{\mathcal{NN}}$, i.e., we consider the following discretization of Problem (2.6): Find $u^{\mathcal{NN}} \in U^{\mathcal{NN}}$ such that

$$u^{\mathcal{NN}} \in \arg \min_{w \in U^{\mathcal{NN}}} R_h^2(w). \quad (3.12)$$

Note that the solution $u^{\mathcal{NN}}$ may not be unique; however, a suitable choice of the space U_H may lead to the control of the error $u - \mathcal{I}_H Bu^{\mathcal{NN}}$ in the H^1 -norm, as we will see in the sequel.

Remark 3.1 (Discretization without interpolation). For the sake of comparison, we will also consider the optimization problem in which no interpolation is applied to the neural network functions. In other words, the target equations are those in (3.6), which induce the following definition of loss function

$$\hat{R}_h^2(w) = \sum_{i \in I_h} \hat{r}_{h,i}^2(w) \gamma_i^{-1}, \quad \text{with} \quad \hat{r}_{h,i}(w) = F_h(\varphi_i) - a_h(Bw, \varphi_i), \quad (3.13)$$

and the following minimization problem: Find $\hat{u}^{\mathcal{NN}} \in U^{\mathcal{NN}}$ such that

$$\hat{u}^{\mathcal{NN}} \in \arg \min_{w \in U^{\mathcal{NN}}} \hat{R}_h^2(w). \quad (3.14)$$

Note that in this problem the triangulation \mathcal{T}_H and the space U_H play no role. Although we will not provide a rigorous error analysis for such discretization, it will be interesting to numerically compare the behavior of the approaches (i.e., with or without interpolation). This will be done in Section 6.

4 A priori error estimates

Let $u^{\mathcal{NN}} \in U^{\mathcal{NN}}$ be any solution of the minimization problem (3.12); let us set

$$u_H^{\mathcal{NN}} = \mathcal{I}_H B u^{\mathcal{NN}} \in U_H. \quad (4.1)$$

Recalling the definition (2.4) of the affine mapping B , it holds

$$u_H^{\mathcal{NN}} = \bar{u}_H + u_H^{\mathcal{NN},0}, \quad \text{with} \quad \bar{u}_H = \mathcal{I}_H \bar{u} \quad \text{and} \quad u_H^{\mathcal{NN},0} = \mathcal{I}_H(\Phi u^{\mathcal{NN}}) \in U_{H,0}; \quad (4.2)$$

note that \bar{u}_H is a discrete lifting in U_H of the Dirichlet data g .

We aim at estimating the error between u and $u_H^{\mathcal{NN}}$. To accomplish this task, we need several definitions, assumptions, and technical results.

Definition 4.1 (norm-equivalence). Let us denote by $0 < c_h \leq C_h$ the constants in the norm equivalence

$$c_h \|v_h\|_{1,\Omega} \leq \|v\|_\gamma \leq C_h \|v_h\|_{1,\Omega} \quad \forall v_h \in V_h, \quad (4.3)$$

where $v = (v_i)_{i \in I_h}$ is such that $v_h = \sum_{i \in I_h} v_i \varphi_i$, and $\|v\|_\gamma = (\sum_{i \in I_h} v_i^2 \gamma_i)^{1/2}$.

Next, we introduce the consistency errors due to numerical quadratures

$$E_h^a(w_H, v_h) = a(w_H, v_h) - a_h(w_H, v_h) \quad \forall w_H \in U_H, \forall v_h \in V_h, \quad (4.4)$$

$$E_h^F(v_h) = F(v_h) - F_h(v_h) \quad \forall v_h \in V_h, \quad (4.5)$$

and we provide a bound on these errors. To this end, let us assume that the quadrature rules used in the elements in \mathcal{T}_h are obtained by affine transformations from a quadrature rule $\{(\hat{\xi}_\iota, \hat{\omega}_\iota) : \iota \in \hat{I}\}$ on a reference element $\hat{E} \subset \mathbb{R}^n$; similarly, let us assume that the quadrature rules used in the edges on $\partial \mathcal{T}_h(\Gamma_N)$ are obtained by affine transformations from a quadrature rule $\{(\check{\xi}_\iota, \check{\omega}_\iota) : \iota \in \check{I}\}$ on a reference element $\check{e} \subset \mathbb{R}^{n-1}$.

Assumption 4.2 (Data smoothness). Let us assume the following smoothness of data:

$$\mu, \sigma, f \in W^{k,\infty}(\Omega), \quad \beta \in (W^{k,\infty}(\Omega))^n, \quad \psi \in W^{k,\infty}(\Gamma_N), \quad (4.6)$$

where k is an integer satisfying

$$1 \leq k \leq k_{\text{int}} = q + 2 - k_{\text{test}}. \quad (4.7)$$

Consequently, let us introduce the following notation

$$\mathcal{N}_k(\mu, \beta, \sigma) = \|\mu\|_{W^{k,\infty}(\Omega)} + \|\beta\|_{(W^{k,\infty}(\Omega))^n} + \|\sigma\|_{W^{k,\infty}(\Omega)}, \quad (4.8)$$

$$\mathcal{N}_k(f, \psi) = \|f\|_{W^{k,\infty}(\Omega)} + \|\psi\|_{W^{k,\infty}(\Gamma_N)}, \quad (4.9)$$

$$\|w_H\|_{k,\mathcal{T}_H} = \left(\sum_{G \in \mathcal{T}_H} \|w_H|_G\|_{H^k(G)} \right)^{1/2} \quad \forall w_H \in U_H. \quad (4.10)$$

Property 4.3 (approximation of the forms a and F). Under Assumption 4.2, it holds

$$|E_h^a(w_H, v_h)| \lesssim h^k \mathcal{N}_k(\mu, \beta, \sigma) \|w_H\|_{k,\mathcal{T}_H} \|v_h\|_{1,\Omega} \quad \forall w_H \in U_H, \forall v_h \in V_h, \quad (4.11)$$

$$|E_h^F(v_h)| \lesssim h^k \mathcal{N}_k(f, \psi) \|v_h\|_{1,\Omega} \quad \forall v_h \in V_h, \quad (4.12)$$

Proof. Both estimates are classical in the theory of finite elements (see, e.g., [2]). As far as (4.11) is concerned, the standard proof given for the case in which the polynomial degree is the same for both arguments, i.e., $k = k_{\text{test}} \geq 1$ and $q = 2(k - 1)$, can be easily adapted to the present situation $k + k_{\text{test}} \leq q + 2$. In this way, one gets $|E_h^a(w_H, v_h)| \lesssim h^k \mathcal{N}_k(\mu, \beta, \sigma) \|w_H\|_{k, \mathcal{T}_h} \|v_h\|_{1, \Omega}$, and one concludes by observing that $\|w_H\|_{k, \mathcal{T}_h} = \|w_H\|_{k, \mathcal{T}_H}$ since \mathcal{T}_h is a refinement of \mathcal{T}_H . \square

Finally, we pose a fundamental assumption.

Assumption 4.4 (inf-sup condition between $U_{H,0}$ and V_h). *The bilinear form a satisfies an inf-sup condition with respect to the spaces $U_{H,0}$ and V_h , namely there exists a constant $\alpha_\star > 0$, independent of the meshsizes h and H , such that*

$$\alpha_\star \|w_H\|_{1, \Omega} \leq \sup_{v_h \in V_h} \frac{a(w_H, v_h)}{\|v_h\|_{1, \Omega}} \quad \forall w_H \in U_{H,0}. \quad (4.13)$$

This assumption together with Property 4.3 yields the following result.

Proposition 4.5 (discrete inf-sup condition between $U_{H,0}$ and V_h). *Under Assumptions 4.2 and 4.4, for all $h \leq h_0$ small enough the bilinear form a_h satisfies an inf-sup condition with respect to the spaces $U_{H,0}$ and V_h , namely there exists a constant $\tilde{\alpha}_\star > 0$ such that*

$$\tilde{\alpha}_\star \|w_H\|_{1, \Omega} \leq \sup_{v_h \in V_h} \frac{a_h(w_H, v_h)}{\|v_h\|_{1, \Omega}} \quad \forall w_H \in U_{H,0}. \quad (4.14)$$

Proof. We have $a_h(w_H, v_h) = a(w_H, v_h) - E_h^a(w_H, v_h)$. Using the bound (4.11) with $k = 1$ and observing that $\|w_H\|_{1, \mathcal{T}_H} = \|w_H\|_{1, \Omega}$, one can find $h_0 > 0$ small enough such that, for all $h \leq h_0$, $|E_h^a(w_H, v_h)| \leq \frac{1}{2} \alpha_\star \|w_H\|_{1, \Omega} \|v_h\|_{1, \Omega}$, whence the result with $\tilde{\alpha}_\star = \frac{1}{2} \alpha_\star$. \square

We are ready to estimate the error $\|u - u_H^{\mathcal{NN}}\|_{1, \Omega}$. Recalling the decomposition (4.2), we use the triangle inequality

$$\|u - u_H^{\mathcal{NN}}\|_{1, \Omega} \leq \|u - u_H\|_{1, \Omega} + \|u_H - u_H^{\mathcal{NN}}\|_{1, \Omega}, \quad (4.15)$$

where u_H is a suitable element in the affine subspace $\bar{u}_H + U_{H,0} \subset U_H$. Writing $u_H = \bar{u}_H + u_{H,0}$ with $u_{H,0} \in U_{H,0}$, one has $u_H - u_H^{\mathcal{NN}} = u_{H,0} - u_{H,0}^{\mathcal{NN}} \in U_{H,0}$; hence, we can apply (4.14) to get

$$\|u_H - u_H^{\mathcal{NN}}\|_{1, \Omega} \leq \frac{1}{\tilde{\alpha}_\star} \sup_{v_h \in V_h} \frac{a_h(u_H - u_H^{\mathcal{NN}}, v_h)}{\|v_h\|_{1, \Omega}}. \quad (4.16)$$

Recalling the definitions (4.11) and (4.5), it holds

$$\begin{aligned} a_h(u_H, v_h) &= a(u_H, v_h) - E_h^a(u_H, v_h) \\ &= a(u, v_h) - a(u - u_H, v_h) - E_h^a(u_H, v_h) \\ &= F(v_h) - a(u - u_H, v_h) - E_h^a(u_H, v_h) \\ &= F_h(v_h) + E_h^F(v_h) - a(u - u_H, v_h) - E_h^a(u_H, v_h). \end{aligned}$$

Thus, the numerator in (4.16) is given by

$$a_h(u_H - u_H^{\mathcal{NN}}, v_h) = F_h(v_h) - a_h(u_H^{\mathcal{NN}}, v_h) - a(u - u_H, v_h) - E_h^a(u_H, v_h) + E_h^F(v_h).$$

On the other hand, recalling (3.10) we have

$$F_h(v_h) - a_h(u_H^{\mathcal{NN}}, v_h) = F_h(v_h) - a_h(\mathcal{I}_H B u^{\mathcal{NN}}, v_h) = \sum_{i \in I_h} r_{h,i}(u^{\mathcal{NN}}) v_i, \quad (4.17)$$

hence, by (3.11) and (4.3),

$$|F_h(v_h) - a_h(u_H^{\mathcal{NN}}, v_h)| \leq R_h(u^{\mathcal{NN}}) \|v\|_\gamma \leq C_h R_h(u^{\mathcal{NN}}) \|v_h\|_{1, \Omega}.$$

Using the bounds (4.11) and (4.12), we obtain the following inequality

$$\begin{aligned} \|u - u_H^{\mathcal{NN}}\|_{1, \Omega} &\lesssim \left(1 + \frac{1}{\tilde{\alpha}_\star}\right) \left(\inf_{u_H \in \bar{u}_H + U_{H,0}} (\|u - u_H\|_{1, \Omega} + h^k \mathcal{N}_k(\mu, \beta, \sigma) \|u_H\|_{k, \mathcal{T}_H}) \right. \\ &\quad \left. + C_h R_h(u^{\mathcal{NN}}) + h^k \mathcal{N}_k(f, \psi) \right). \end{aligned} \quad (4.18)$$

From now on, we assume that $u \in H^{k+1}(\Omega)$. Then, assumption (3.8) yields the inequalities

$$\|u - \mathcal{I}_H u\|_{1,\Omega} \lesssim H^k |u|_{k+1,\Omega} \lesssim h^k |u|_{k+1,\Omega} \quad (4.19)$$

and

$$\|\mathcal{I}_H u\|_{k,\mathcal{T}_H} \leq \|u\|_{k,\Omega} + \|u - \mathcal{I}_H u\|_{k,\mathcal{T}_H} \lesssim \|u\|_{k,\Omega} + H |u|_{k+1,\Omega} \lesssim \|u\|_{k+1,\Omega}. \quad (4.20)$$

Choosing $u_H = \mathcal{I}_H u \in \bar{u}_H + U_{H,0}$ in (4.18) and using these estimates, we arrive at the following intermediate result.

Lemma 4.6. *Under the previous assumptions, it holds*

$$\|u - u_H^{\mathcal{NN}}\|_{1,\Omega} \lesssim h^k (|u|_{k+1,\Omega} + \mathcal{N}_k(\mu, \beta, \sigma) \|u\|_{k+1,\Omega} + \mathcal{N}_k(f, \psi)) + C_h R_h(u^{\mathcal{NN}}).$$

Our next task will be bounding the term $R_h(u^{\mathcal{NN}})$. To this end, we use the minimality condition (3.12) to get

$$R_h(u^{\mathcal{NN}}) \leq R_h(w^{\mathcal{NN}}) \quad \forall w^{\mathcal{NN}} \in U^{\mathcal{NN}}. \quad (4.21)$$

On the other hand, since $R_h(w^{\mathcal{NN}})$ is a weighted ℓ_2 -norm in $\mathbb{R}^{|I_h|}$, we can write

$$R_h(w^{\mathcal{NN}}) = \sup_{\mathbf{z} \in \mathbb{R}^{|I_h|}} \frac{1}{\|\mathbf{z}\|_\gamma} \sum_{i \in I_h} r_{h,i}(w^{\mathcal{NN}}) z_i,$$

where, similarly to (4.17),

$$\sum_{i \in I_h} r_{h,i}(w^{\mathcal{NN}}) z_i = F_h(z_h) - a_h(\mathcal{I}_H B w^{\mathcal{NN}}, z_h) \quad \text{with } z_h = \sum_{i \in I_h} z_i \varphi_i \in V_h.$$

For convenience, in analogy with (4.1), let us set

$$w_H^{\mathcal{NN}} = \mathcal{I}_H B w^{\mathcal{NN}} \in U_H. \quad (4.22)$$

Thus, recalling (4.3), we obtain

$$R_h(w^{\mathcal{NN}}) \leq \frac{1}{c_h} \sup_{z_h \in V_h} \frac{F_h(z_h) - a_h(w_H^{\mathcal{NN}}, z_h)}{\|z_h\|_{1,\Omega}} \quad \forall w^{\mathcal{NN}} \in U^{\mathcal{NN}}. \quad (4.23)$$

The numerator can be manipulated as above, using

$$F_h(z_h) = F(z_h) - E_h^F(z_h) = a(u, z_h) - E_h^F(z_h)$$

and

$$a_h(w_H^{\mathcal{NN}}, z_h) = a(w_H^{\mathcal{NN}}, z_h) - E_h^a(w_H^{\mathcal{NN}}, z_h),$$

whence, using once more Property 4.3, we get

$$R_h(w^{\mathcal{NN}}) \lesssim \frac{1}{c_h} (\|u - w_H^{\mathcal{NN}}\|_{1,\Omega} + h^k \mathcal{N}_k(\mu, \beta, \sigma) \|w_H^{\mathcal{NN}}\|_{k,\mathcal{T}_H} + h^k \mathcal{N}_k(f, \psi)). \quad (4.24)$$

In order to bound the terms containing $w_H^{\mathcal{NN}}$, we introduce the quantity

$$e^{\mathcal{NN}} = u - B w^{\mathcal{NN}}, \quad (4.25)$$

which, recalling the definitions (2.4) and (2.5), can be written by as

$$e^{\mathcal{NN}} = \Phi(\tilde{u} - w^{\mathcal{NN}}), \quad (4.26)$$

and we formulate a final assumption.

Assumption 4.7 (smoothness of the solution and the neural network manifold). *The solution u can be represented as in (2.4) with*

$$\tilde{u} \in H^{k+1}(\Omega) \quad \text{and} \quad \Phi \in W^{k+1,\infty}(\Omega) \quad (4.27)$$

for k satisfying (4.7). Furthermore, the manifold formed by the neural network functions satisfies the smoothness condition

$$U^{\mathcal{NN}} \subset H^2(\Omega). \quad (4.28)$$

Note that (4.27) implies in particular $u \in H^{k+1}(\Omega)$ with $\|u\|_{k+1,\Omega} \lesssim \|\tilde{u}\|_{k+1,\Omega} \|\Phi\|_{k+1,\infty,\Omega}$; on the other hand, (4.28) implies $e^{\mathcal{NN}} \in H^2(\Omega)$. (We refer to Remark 4.11 for another set of assumptions on the neural network.)

Recalling (4.22) and using the identity

$$u - w_H^{\mathcal{NN}} = (u - \mathcal{I}_H u) + \mathcal{I}_H e^{\mathcal{NN}} = (u - \mathcal{I}_H u) - e^{\mathcal{NN}} + (I - \mathcal{I}_H) e^{\mathcal{NN}}, \quad (4.29)$$

we can write

$$\|u - w_H^{\mathcal{NN}}\|_{1,\Omega} \lesssim \|u - \mathcal{I}_H u\|_{1,\Omega} + \|e^{\mathcal{NN}}\|_{1,\Omega} + H|e^{\mathcal{NN}}|_{2,\Omega} \quad (4.30)$$

and, using a standard inverse inequality in $\mathbb{P}_k(G)$ for any $G \in \mathcal{T}_H$,

$$\begin{aligned} \|w_H^{\mathcal{NN}}\|_{k,\mathcal{T}_H} &\lesssim \|\mathcal{I}_H u\|_{k,\mathcal{T}_H} + H^{1-k} \|\mathcal{I}_H e^{\mathcal{NN}}\|_{1,\Omega} \\ &\lesssim \|\mathcal{I}_H u\|_{k,\mathcal{T}_H} + H^{1-k} (\|e^{\mathcal{NN}}\|_{1,\Omega} + H|e^{\mathcal{NN}}|_{2,\Omega}). \end{aligned} \quad (4.31)$$

Keeping into account (4.19) and (4.20), in order to conclude we need to identify a function $\tilde{w}^{\mathcal{NN}} \in U^{\mathcal{NN}}$ for which a bound of the type

$$|e^{\mathcal{NN}}|_{m,\Omega} \lesssim |\tilde{u} - \tilde{w}^{\mathcal{NN}}|_{m,\Omega} \lesssim H^{k+1-m} |\tilde{u}|_{k+1,\Omega} \quad (4.32)$$

holds true for $m = 1, 2$. The existence of such a function is guaranteed by one of the available results on the approximation of functions in Sobolev spaces by neural networks (see [3, Theorem 5.1, Remark 5.2]; see also [18]), provided the number of layers L and the widths of the layers in the chosen \mathcal{NN} satisfy suitable conditions depending on the target accuracy (hence, in our case depending on H^k).

Substituting (4.32) into (4.30) and (4.31), and using inequalities (4.21) and (4.24), we arrive at the following bound on the loss $R_h(u^{\mathcal{NN}})$.

Lemma 4.8. *Under the previous assumptions, it holds*

$$R_h(u^{\mathcal{NN}}) \lesssim \frac{1}{c_h} (H^k |u|_{k+1,\Omega} + H^k |\tilde{u}|_{k+1,\Omega} + h^k \mathcal{N}_k(\mu, \beta, \sigma) \|\tilde{u}\|_{k+1,\Omega} + h^k \mathcal{N}_k(f, \psi)).$$

Concatenating Lemmas 4.6 and 4.8, and using once more $H \lesssim h$, we obtain the following a priori error estimate for the solution of Problem (3.12).

Theorem 4.9 (a priori error estimate). *Let $u_H^{\mathcal{NN}} \in U_H$ be defined by (4.1). Under Assumptions 4.2, 4.4 and 4.7, for h sufficiently small it holds*

$$\|u - u_H^{\mathcal{NN}}\|_{1,\Omega} \lesssim \left(1 + \frac{C_h}{c_h}\right) h^k [(1 + \mathcal{N}_k(\mu, \beta, \sigma)) \|\tilde{u}\|_{k+1,\Omega} + \mathcal{N}_k(f, \psi)]. \quad (4.33)$$

Remark 4.10 (on the equivalence constants c_h, C_h). If a classical Lagrange basis is used in (3.10), and the triangulation \mathcal{T}_h is quasi-uniform, then for constants weights $\gamma_i = 1$ one has $c_h \simeq h^{1-d/2}$ and $C_h \simeq h^{-d/2}$, whence $\frac{C_h}{c_h} \simeq h^{-1}$. On the other hand, if a hierarchical basis is used instead, then $c_h \simeq C_h \simeq 1$, hence, $\frac{C_h}{c_h} \simeq 1$ in dimension $d = 1$, whereas $c_h \simeq |\log h|^{-1}$, $C_h \simeq 1$, hence, $\frac{C_h}{c_h} \simeq |\log h|$ in dimension $d = 2$.

Thus, the presence of the ratio $\frac{C_h}{c_h}$ in (4.33), which originates from the control of the loss function, makes this estimate sub-optimal. However, our numerical experiments in Sect. 6 indicate that this adverse effect is only seen with certain combinations of the discretization parameters and not with others. The reason of the different behavior may be traced back to the fact that when we compare the value $R_h(u^{\mathcal{NN}})$ of the loss function obtained by minimization to that of $R_h(\tilde{w}^{\mathcal{NN}})$, where \tilde{w} is an approximation of \tilde{u} satisfying (4.32), not only it holds $R_h(u^{\mathcal{NN}}) \leq R_h(\tilde{w}^{\mathcal{NN}})$ as predicted by (4.21) but in some cases the stronger inequality

$$\frac{C_h}{c_h} R_h(u^{\mathcal{NN}}) \leq R_h(\tilde{w}^{\mathcal{NN}}), \quad (4.34)$$

holds true, which clearly allows us to drop the factor $\frac{C_h}{c_h}$ in (4.33). We refer to Sect. 6.4 for more details. \square

Remark 4.11 (low-regularity \mathcal{NN}). When the condition $U^{\mathcal{NN}} \subset H^2(\Omega)$ fails to be satisfied, as for the ReLU activation function, we may provide a different set of assumptions which still lead to an $O(h^k)$ -error estimate as in Theorem 4.9. Precisely, we may assume that $\tilde{u} \in W^{k+1,\infty}(\Omega)$ and $U^{\mathcal{NN}} \subset W^{1,\infty}(\Omega)$. Then, referring to the first equality in (4.29), one has

$$\|u - w_H^{\mathcal{NN}}\|_{1,\Omega} \leq \|(u - \mathcal{I}_H u)\|_{1,\Omega} + \|\mathcal{I}_H e^{\mathcal{NN}}\|_{1,\Omega} \lesssim \|(u - \mathcal{I}_H u)\|_{1,\Omega} + H^{-1} \|\mathcal{I}_H e^{\mathcal{NN}}\|_{0,\Omega},$$

with

$$\begin{aligned}\|\mathcal{I}_H e^{\mathcal{NN}}\|_{0,\Omega}^2 &= \sum_{G \in \mathcal{T}_H} \|\mathcal{I}_H e^{\mathcal{NN}}\|_{0,G}^2 \leq \sum_{G \in \mathcal{T}_H} \|\mathcal{I}_H e^{\mathcal{NN}}\|_{L^\infty(G)}^2 |G| \\ &\lesssim \sum_{G \in \mathcal{T}_H} \|e^{\mathcal{NN}}\|_{L^\infty(G)}^2 |G| \lesssim H^d \|e^{\mathcal{NN}}\|_{L^\infty(\Omega)}^2.\end{aligned}$$

The conclusion easily follows if $\tilde{w}^{\mathcal{NN}}$ is chosen to satisfy the error bound $\|\tilde{u} - \tilde{w}^{\mathcal{NN}}\|_{L^\infty(\Omega)} \lesssim H^{k+1} |\tilde{u}|_{W^{k+1,\infty}(\Omega)}$, which is possible according to the results in [7], [17]. \square

5 Implementation issues

As specified in Section 3.1, we use a fully-connected feed-forward neural network architecture, which is fixed and depends neither on the PDE nor on its discretization. For each test case, we initialize the neural network with a completely new set of weights, which is important to show that our results are not initialization dependent. The activation function is the hyperbolic tangent. It has been proven in [3] that such neural networks with two hidden layers enjoy exponential converge properties with respect to the number of weights. Nevertheless, in order to simplify the training and enrich the space in which we seek the numerical solution, we consider four layers (namely, $L = 4$ with the notation of Section 3.1) with 50 neurons each ($N_\ell = 50$, $\ell = 1, \dots, 4$). We also highlight that it is always possible to approximate the identity function with a neural network with a single layer with just one neuron. The best approximation obtainable with a neural network with more than two layers is thus more accurate than the one computable with a neural network with just two layers, because, in the worst possible case, the L -layers neural network can be obtained combining an $(L - 2)$ -layers identity neural network with a suitable 2-layers neural network.

In order to compute the results shown in Section 6, we compare various state of the art optimizers to find the most efficient way to minimize, as much as possible, the loss function. We observe that most of the momentum based first order methods have similar performances (the results are computed with the Yogi optimizer [20]) but that it is convenient to use a learning rate scheduler in order to reduce the learning during the process. We tested both cyclical learning rate schedulers and exponential learning rate schedulers [25], the differences were very subtle and we thus choose to adopt the most common exponential learning rate scheduler and decided not to report images about such a comparison. To further reduce the loss function, in order to obtain a solution that is as close as possible to a global minimizer, we also use the BFGS method and its limited-memory version: the L-BFGS method [29].

The Dirichlet boundary conditions are imposed via the mapping B defined in (2.5). The construction of the function Φ is particularly simple when Ω is a convex polygon, since in this case Φ can be defined as the product of the linear polynomials which vanish on each Dirichlet edge; this in precisely how we define Φ in the numerical examples discussed in the next session. In other geometries, one can build Φ by using a level-set method, or even by training an auxiliary neural network to (approximately) vanish on Γ_D . Similarly, if no extension \bar{u} of the Dirichlet data g is known analytically, one can train another neural network to (approximately) match the values of g on Γ_D .

5.1 VPINN efficiency and the inf-sup condition

In Sect. 3 we introduced a discretization method in which the loss function is built by a piecewise polynomial interpolation of the neural network; on the other hand, we also mentioned in Remark 3.1 the possibility of building the loss function directly from the (non-interpolated) neural network. In the next section, we will provide numerical results for both approaches.

From the theoretical point of view, only the former approach can be considered mathematically reliable, since the error control is based on the validity of an inf-sup condition, as detailed in Sect. 4. On the contrary, if the neural network is used without interpolation, one usually gets an under-determined system, for which the error control may be problematic; consider, for instance, that the discrete solution with zero data may not be identically zero, as documented in Sect. 6.3, which rules out uniqueness. Nonetheless, there is empirical evidence (see, e.g., [32, 22, 9, 28]) that non-interpolated neural networks do succeed in computing accurate solutions even in complex scenarios. Actually, in the next section we will provide numerical evidence that the two approaches are always (in the considered cases) comparable in terms of rate of convergence and, in most cases, smaller errors are obtained without interpolation.

From the computational point of view, the two approaches have comparable advantages and disadvantages. Let us first consider non-interpolated neural networks. The corresponding loss functions can be more easily implemented thanks to the existing deep-learning frameworks, which allow the direct computation of neural network derivatives via automatic differentiation [1]. One only needs to generate a mesh and the corresponding test functions, associate a quadrature rule to each element and assemble all the tensors required to efficiently compute the loss function. The main difference with the interpolated neural network approach is that, in the latter, the interpolation matrices have to be assembled too, although automatic differentiation is not required. Depending on the problem at hand, this may be an advantage or a disadvantage. Indeed, the interpolation matrices assembly may be tricky but, using them, all the

derivatives can be efficiently computed by matrix-vector multiplications that are much cheaper than the entire automatic differentiation procedure, especially when higher order derivatives are required. Therefore, for fast-converging optimization processes, a non-interpolated neural network approach may be efficient and can be more easily implemented; otherwise each optimization step may be much more expensive than the analogous operation performed with an interpolated neural network. Furthermore, we observed that the training phase is much faster when the neural network is interpolated because the procedure converges in fewer steps. This is probably related to the fact that the solution is sought in a significantly smaller space, that can be more easily explored during the training phase.

6 Numerical results

In this section we present several numerical results concerning the VPINN discretization of Problem (2.1) in the interval $\Omega = (0, 1)$ (Sect. 6.1) or in the square $\Omega = (0, 1)^2$ (Sect. 6.2). We will vary the coefficients of the operator, the boundary conditions and the smoothness of the exact solution. For each test case, we vary the degree k_{test} of the test functions, the order q of the quadrature rule (which may be of Gaussian or Newton-Cotes type), and correspondingly we choose the polynomial degree k of the interpolating functions as $k = k_{\text{int}} = q + 2 - k_{\text{test}}$, according to (4.7). Since the theoretical results in Sect. 4 suggest that it is convenient to maintain k_{test} as low as possible, we only use piecewise linear ($k_{\text{test}} = 1$) or piecewise quadratic ($k_{\text{test}} = 2$) test functions. Recalling condition (3.3), we thus choose $q = 3$ or 5 if $k_{\text{test}} = 1$, and $q = 5$ if $k_{\text{test}} = 2$. In other words, for each test case we will show three convergence plots, from left to right, corresponding to the three combinations of parameters

$$\begin{aligned} P_1 &= (q = 3, k_{\text{test}} = 1, k_{\text{int}} = 4) \\ P_2 &= (q = 5, k_{\text{test}} = 1, k_{\text{int}} = 6) \\ P_3 &= (q = 5, k_{\text{test}} = 2, k_{\text{int}} = 5). \end{aligned} \tag{6.1}$$

In all but one case, we build a manufactured exact solution from the smooth function

$$U(t) = \cos 5t + t^2, \tag{6.2}$$

by setting $u(x) = U(x)$ in one-dimensional problems and $u(x, y) = U(x + \frac{1}{2}y)$ in two-dimensional problems. Just in one test case, we use a non-smooth exact solution, belonging to $H^1(\Omega)$ but not to $H^2(\Omega)$.

In each plot we report by black dots the error $\|u - u_H^{\mathcal{NN}}\|_{1,\Omega}$, where $u_H^{\mathcal{NN}}$ is the interpolated neural network defined on the mesh \mathcal{T}_H as in (4.1), versus the size h of the mesh \mathcal{T}_h supporting the test functions used for the training process. In order to satisfy the discrete inf-sup condition, we choose \mathcal{T}_H and \mathcal{T}_h as nested meshes whose meshsizes satisfy $H = k_{\text{int}}h$. A pair of meshes $(\mathcal{T}_H, \mathcal{T}_h)$, used in Sect. 6.2, is represented in Fig. 1 together with the elemental refinement corresponding to $k_{\text{int}} = 4$, $k_{\text{int}} = 5$ and $k_{\text{int}} = 6$. We also show a black solid line and a black dashed one: the former is the regression line fitting the black dots (possibly ignoring the first ones); its slope in the log-log plane yields the empirical convergence rate. The latter is used as a reference, since its slope corresponds to an error decay proportional to $h^{k_{\text{int}}}$, as indicated by Theorem 4.9 assuming that the ratio $\frac{C_h}{c_h}$ may be neglected (i.e., assuming that condition (4.34) is satisfied); this line represents the best convergence rate we can expect from the proposed discretization scheme.

For comparison, we also report by green dots the error $\|u - \hat{u}^{\mathcal{NN}}\|_{1,\Omega}$, where $\hat{u}^{\mathcal{NN}}$ is the non-interpolated neural network defined in Remark 3.1. Whenever these dots, possibly after a pre-asymptotic phase, sit close to their regression line, we draw it as well in dashed green.

6.1 One-dimensional problems

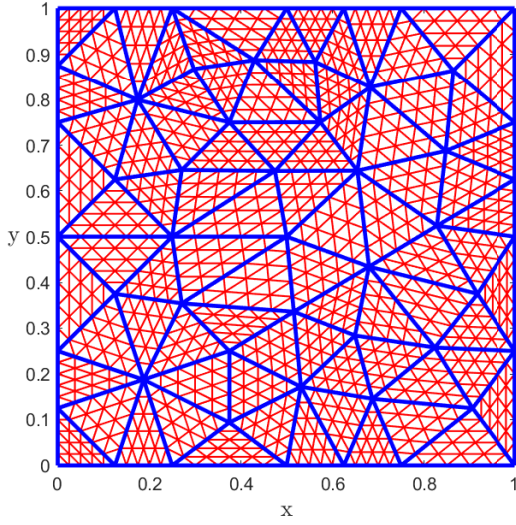
In all subsequent tests, we use a uniform partition \mathcal{T}_h of the interval $\Omega = (0, 1)$; the exact solution u is invariably defined via (6.2), and the boundary conditions are of Dirichlet type at both endpoints.

Test 1

Let us start from the simplest situation, namely we choose $\mu = 1, \beta = 0, \sigma = 0$, and we use Gaussian rules to compute integrals in the loss function. The observed error decays are shown in Fig. 2.

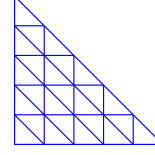
The three plots clearly indicate that the convergence histories are quite regular for the interpolated networks, as the black dots are almost invariably sitting on the corresponding regression lines. This feature will be observed in all the subsequent numerical tests, indicating that interpolation adds a remarkable robustness in the network training.

With the parameter sets P_1 (corresponding to subfigure (2.a)) and P_2 (subfigure (2.b)), the best possible theoretical convergence rate k_{int} is achieved; on the contrary, with the parameter set P_3 (subfigure (2.c)) the observed convergence rate is one order less than the optimal one, thereby indicating that the estimate of Theorem 4.9, in which $\frac{C_h}{c_h} \simeq h^{-1}$, is sharp. This different behavior will be discussed and motivated in Sect. 6.4. Overall, the three plots confirm the theoretical predictions that increasing the order of the quadrature rule improves the convergence rate, whereas increasing the degree of the trial functions reduces the convergence rate.

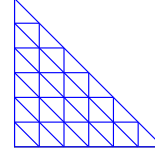


(1.a) Delaunay meshes \mathcal{T}_H (blue lines) and \mathcal{T}_h (red lines).
Refinement corresponding to $k_{int} = 5$.

(1.b) Elemental refinement for $k_{int} = 4$.

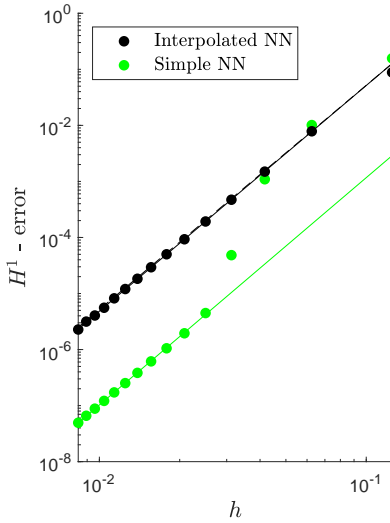


(1.c) Elemental refinement for $k_{int} = 5$.

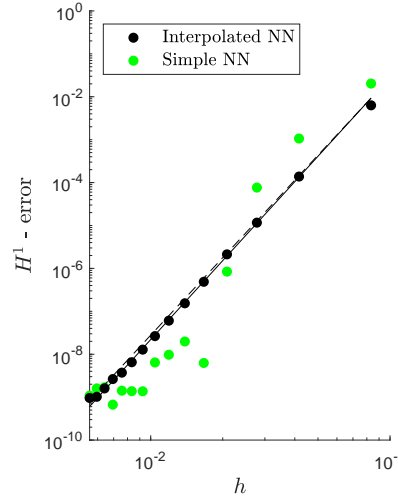


(1.d) Elemental refinement for $k_{int} = 6$.

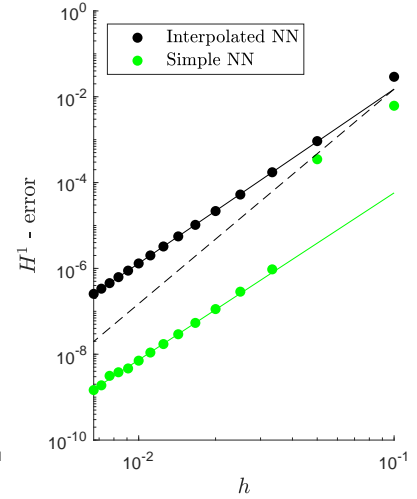
Fig. 1 One of the meshes used in Sect. 6.2 and elemental refinements chosen to obtain \mathcal{T}_h from \mathcal{T}_H .



(2.a) $q = 3, k_{test} = 1, k_{int} = 4$.
Expected decay rate: 4.
Obtained decay rate: 4.03.



(2.b) $q = 5, k_{test} = 1, k_{int} = 6$.
Expected decay rate: 6.
Obtained decay rate: 6.11.



(2.c) $q = 5, k_{test} = 2, k_{int} = 5$.
Expected decay rate: 5.
Obtained decay rate: 4.06.

Fig. 2 Error decays for *Test 1*: $\mu = 1, \beta = 0, \sigma = 0$. Integrals computed via Gaussian quadrature rules.

The comparison with the errors produced by the non-interpolated networks (indicated as ‘simple networks’ in the plots) is quite interesting. For parameter sets P_1 and P_3 , the decays of the green dots essentially replicate those of the black dots, although the former are below the latter: convergence rates are similar, but errors are significantly smaller. For parameter set P_2 , the situation is less clear-cut, due to a rather random behavior of the non-interpolated networks; in addition, the finite precision of the used Tensorflow software prevents convergence to display at full for small values of h .

Test 2

Let us now allow the three coefficients of the operator to be non-zero, and actually smoothly variable in Ω ; to be specific, let us fix $\mu(x) = 2 + \sin x$, $\beta(x) = e^x$, $\sigma(x) = \sqrt{x+1}$. Gaussian formulas are again used. Results are reported in Fig. 3.

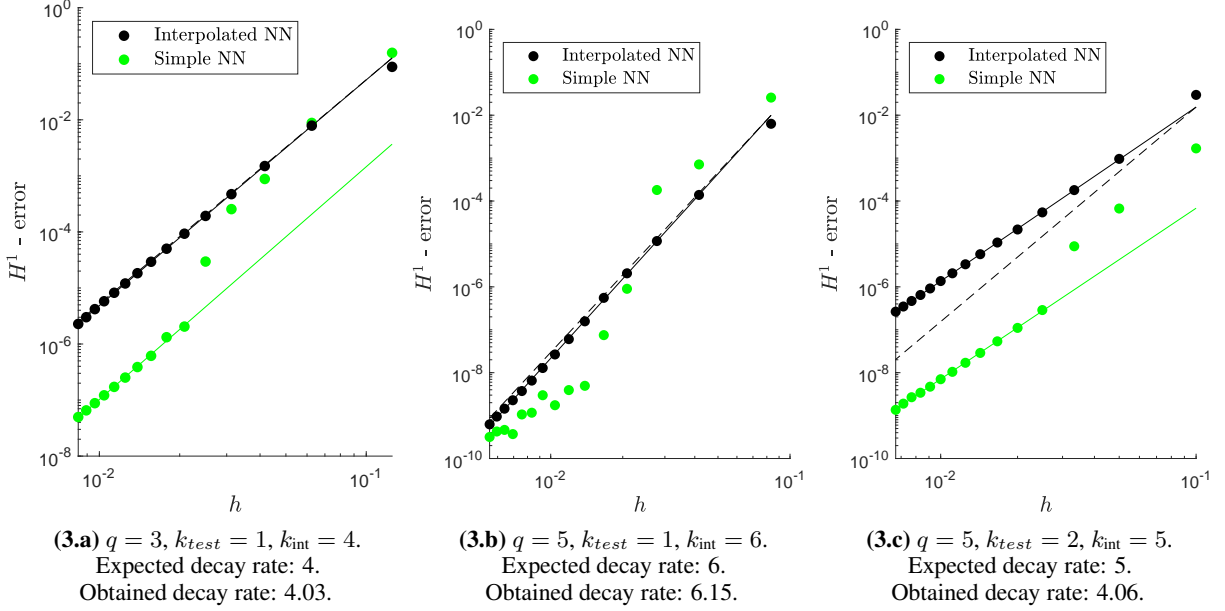


Fig. 3 Error decays for *Test 2*: $\mu(x) = 2 + \sin x$, $\beta(x) = e^x$, $\sigma(x) = \sqrt{x+1}$. Integrals computed via Gaussian quadrature rules.

Note that none of the integrals involved in the residuals evaluations can be exactly computed. Nevertheless, we observe that the error decays hardly differ from the corresponding ones in Fig. 2. This is in full agreement with the theoretical results of Sect. 4.

Test 3

Our last one-dimensional test is devoted to the investigation of the role of the involved quadrature rules. Let us consider the same operator as in *Test 2*, but let us replace each Gaussian formula in the computation of the loss function by a Newton-Cotes formula of the same precision. The obtained numerical results are shown in Fig. 4.

There are no essential differences with respect to Fig. 3 in the behavior of the errors for interpolated networks. For non-interpolated networks, a more pronounced difference can be observed only for parameter set P_2 (subfigure (4.b)), where the error decay is now more regular, as the neural network is evaluated at a larger number of quadrature nodes.

Nearly identical results are observed for both Gaussian and Newton-Cotes rules if the coefficients of the operator are constant.

6.2 Two-dimensional problems

In this section our investigation is extended to two-dimensional problems. We explore the effect of changing meshes, solutions, and boundary conditions. On the other hand, in all tests we use the same set of coefficients, namely $\mu = 1$, $\beta = [2, 3]^T$, $\sigma = 4$, since we observed in one dimension that results are stable to coefficient perturbations. Similarly, we show results for Gaussian integration rules only, since Newton-Cotes rules behave similarly, as observed in one dimension.

Test 4

We consider the smooth solution u defined in $\Omega = (0, 1)^2$ via (6.2), and apply Dirichlet boundary conditions on the whole $\partial\Omega$. Let us initially partition the domain by a uniform triangular grid, obtained by subdividing each square of a uniform tensorial grid into two triangles. The corresponding error behavior is documented in Fig. 5.

The observed convergence histories are qualitatively similar to those in Fig. 3, except that non-interpolated neural network decays are less noisy. For parameter set P_1 (subfigure (5.a)), very close convergence rates are reported: 3.94 for the interpolated network, 4.01 for the non-interpolated one, both very close to the predicted converge rate $k_{int} = 4$. For parameter set P_2 (subfigure (5.b)), the converge rates are 6.00 for the interpolated networks, and 6.46 for the non-interpolated neural networks (the theoretical convergence rate is 6). Note, however, that in this case convergence for the non-interpolated networks was so fast that, in order to avoid numerical troubles due to the Tensorflow finite precision, we had to consider additional meshes \mathcal{T}_h , which are not used with the interpolated networks. At last, for parameter set P_3 (subfigure (5.c)), the black line slope is 4.05, the green line one is 3.97, whereas the optimal convergence rate

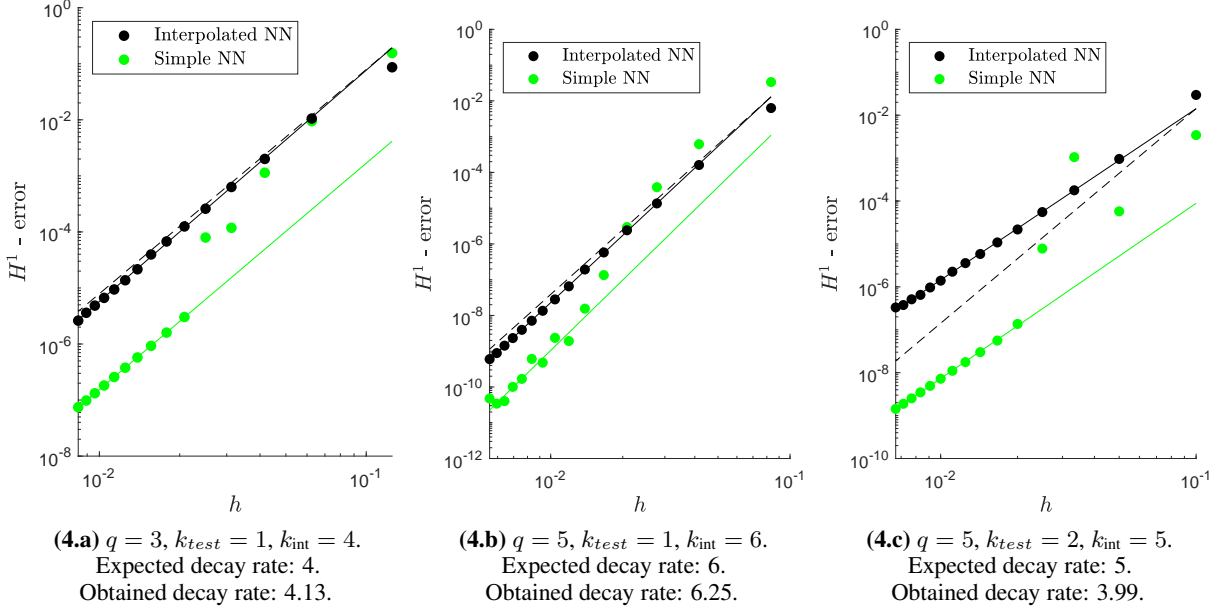


Fig. 4 Error decays for *Test 3*: $\mu(x) = 2 + \sin x$, $\beta(x) = e^x$, $\sigma(x) = \sqrt{x+1}$. Integrals computed via Newton-Cotes quadrature rules.

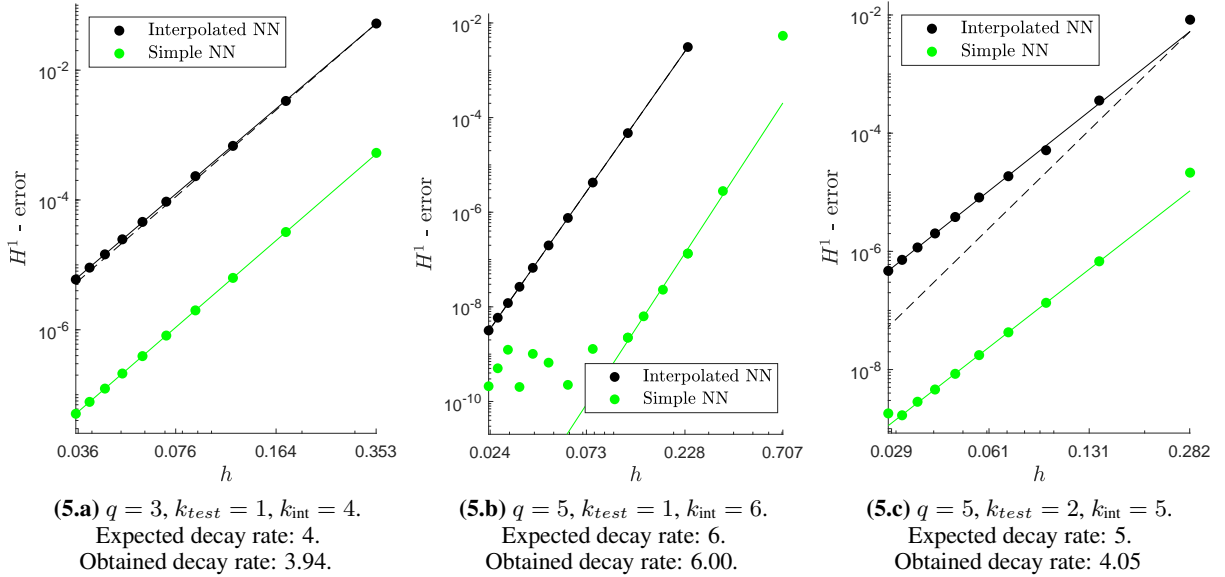


Fig. 5 Error decays for *Test 4*: $\mu = 1$, $\beta = [2, 3]^T$, $\sigma = 4$. Uniform triangular meshes.

is 5. We thus confirm, also in two-dimensional problems, that the presence of the term $\frac{C_h}{c_h} \simeq h^{-1}$ in the estimate of Theorem 4.9 cannot be removed.

We also mention that similar results are obtained if Ω is partitioned into tensorial meshes, and polynomials in \mathbb{Q}_k rather than in \mathbb{P}_k are employed in each element. This choice is not strictly covered by the theory of Sect. 4, although it can be extended in a straightforward manner.

Test 5

Let us now consider generic Delaunay triangular meshes, in which all triangles have approximately the same area. The obtained decays are shown in Fig. 6.

Since the quality of mesh elements may vary from one run to the next one, we expect a more noisy behavior of the errors as compared to those in Fig. 5; this is precisely the case in all plots. Apart from this difference, all convergence

histories are similar to the corresponding ones in *Test 4*; the same caveat applies to the non-interpolated network decay for parameter set P_2 (subfigure (6.b)), for which the measured convergence rate is 6.75.

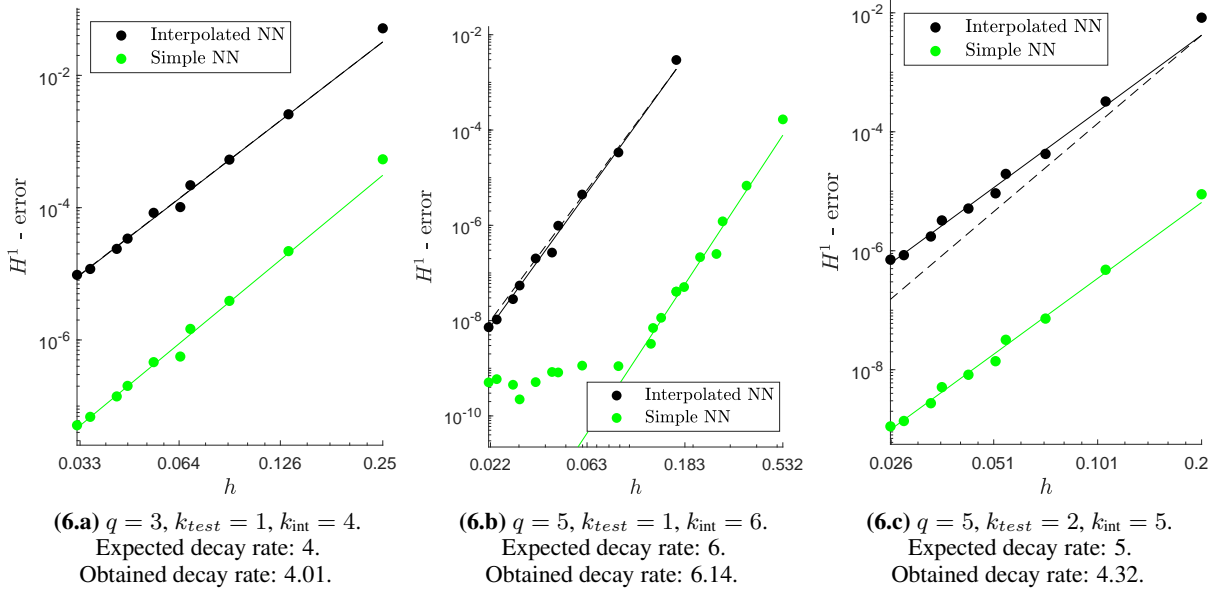


Fig. 6 Error decays for *Test 5*: $\mu = 1, \beta = [2, 3]^T, \sigma = 4$. Delaunay meshes.

Test 6

In order to show that the proposed a priori error estimate is reliable even if the exact solution is not regular, let us consider arbitrary triangular meshes as in *Test 5* and the following exact solution:

$$u(x, y) = U(t) = \begin{cases} \frac{t}{6}, & 0 \leq x < \frac{1}{3}, \\ \frac{t-t^2}{2} - \frac{1}{18}, & \frac{1}{3} \leq t < \frac{2}{3}, \\ \frac{1-t}{6}, & \frac{2}{3} \leq t \leq 1, \end{cases} \quad (6.3)$$

where $t = x + \frac{y}{2}$. Results are reported in Fig. 7.

Since $u \in H^{5/2-\varepsilon}(\Omega)$ for any $\varepsilon > 0$, we expect a convergence rate close to 1.5; indeed, $k_{int} \geq 4$ and the rate of convergence is always limited by the solution regularity. This theoretical prediction is confirmed by the obtained results.

It is worth mentioning that the convergence histories for the interpolated networks maintain a certain stability with respect to the variation of the mesh; this is not the case for the non-interpolated networks, where jumps in errors occur several times. Note as well that for parameter set P_1 (subfigure (7.a)), the interpolated networks are better suited to catch the singularities of the solution, at least in the explored range of variation of the meshsize.

Test 7

Finally, we are interested in proving that changing boundary conditions does not substantially affect the convergence rates. Let us thus choose $\Gamma_D = \{(x, y) \in \partial\Omega : x = 0 \text{ or } x = 1\}$ and $\Gamma_N = \partial\Omega \setminus \Gamma_D$. Let u be again the smooth solution defined via (6.2), and let us use Delaunay triangular grids. The corresponding error decays are represented in Fig. 8.

A comparison with Fig. 6 reveals that the qualitative behavior of the errors is similar. One just observes that numerical issues related to machine precisions decreases the maximum obtainable accuracy for fine meshes.

6.3 On the importance of the inf-sup condition

In this section we show that the inf-sup condition, assumed in Proposition 4.5 to formally derive the a priori estimate, is crucial in order to avoid spurious modes in the numerical solution. To prove such a claim, let us consider the simplest one-dimensional Poisson's problem with zero forcing term and zero Dirichlet boundary conditions:

$$\begin{cases} -\Delta u = 0 & \text{in } \Omega, \\ u = 0 & \text{on } \Gamma_D, \end{cases} \quad (6.4)$$

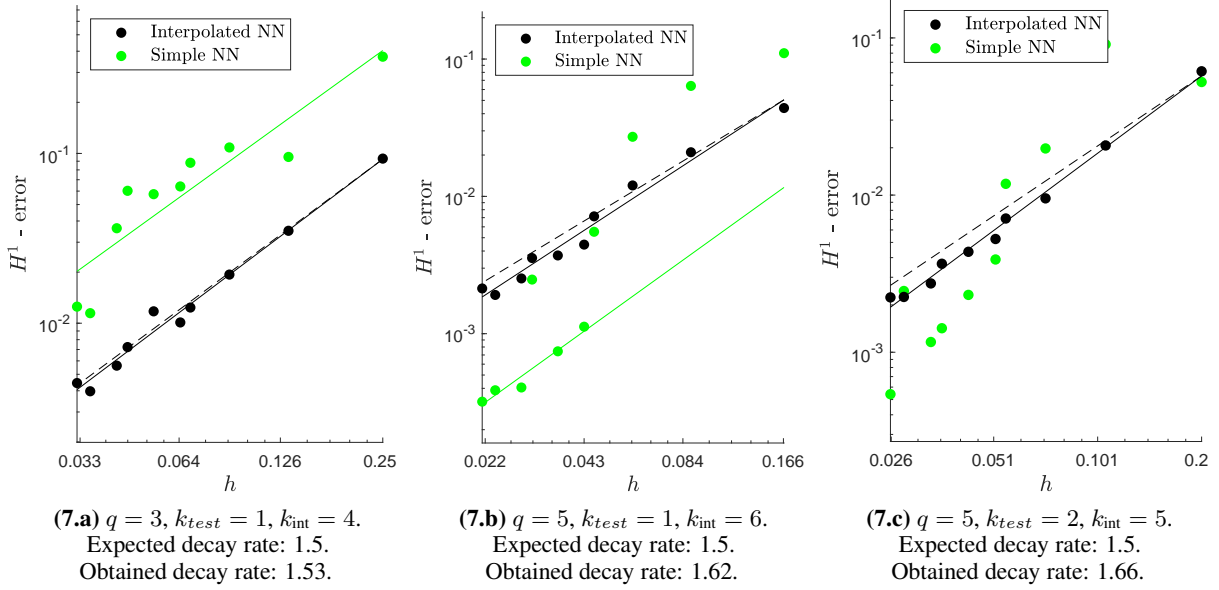


Fig. 7 Error decays for *Test 6*: $\mu = 1, \beta = [2, 3]^T, \sigma = 4$. $u_e \in H^{5/2-\varepsilon}(\Omega)$ for $\varepsilon > 0$. Delaunay meshes.

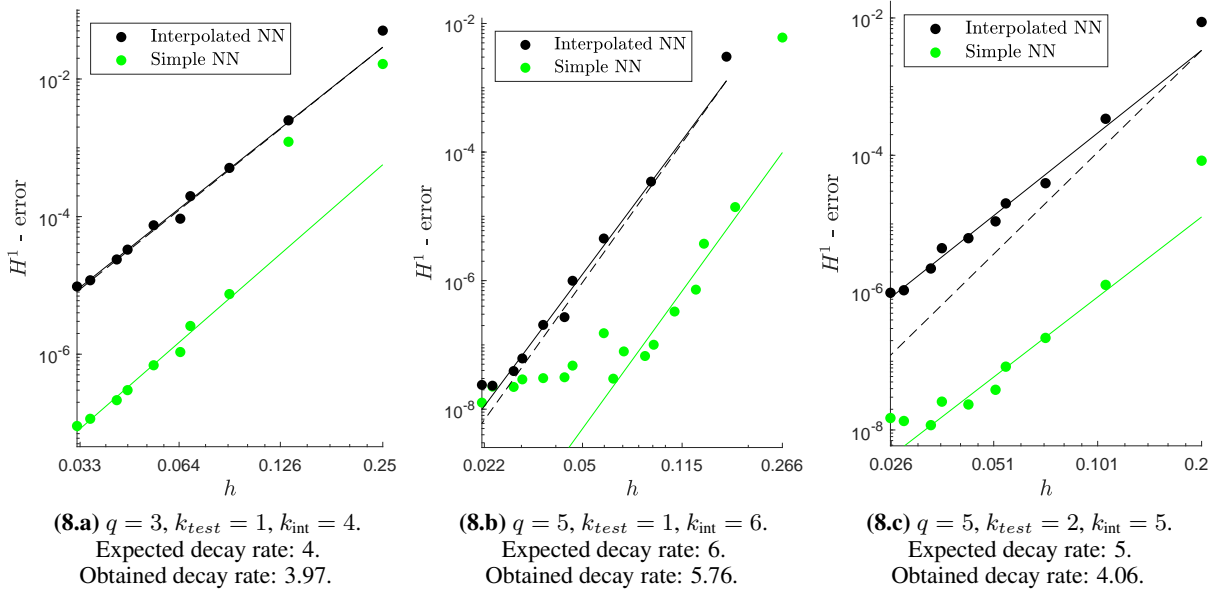


Fig. 8 Error decays for *Test 7*: $\mu = 1, \beta = [2, 3]^T, \sigma = 4$. Delaunay meshes and Neumann boundary conditions.

where $\Omega = (0, 1)$ and $\Gamma_D = \{0, 1\}$. Again for the sake of simplicity, we use the parameter set P_1 . Note that since both $U^{\mathcal{NN}}$ and U_H contain the exact solution $u \equiv 0$, it is always possible to obtain a numerical solution that is identical to the exact one (up to numerical precision).

Let us denote by u_δ any discrete solution defined in Sect. 3.2, namely, either a solution $u_H^{\mathcal{NN}}$ obtained by interpolated neural networks, or a solution $\hat{u}^{\mathcal{NN}}$ obtained by non-interpolated neural networks. These discrete solutions are represented in Fig. 9 in logarithmic scale to allow a direct comparison. In order to avoid numerical issues due to the logarithmic scale of the plot when u_δ gets close to 0, a truncation procedure is applied.

The functions u_δ produced by non-interpolated networks are represented in the left plot of Fig. 9. Each one is obtained by minimizing the loss function up to machine accuracy; despite this, when the mesh is fairly coarse the discrete solution is significantly different from the null solution. Indeed, the initial weights in the training process are non-zero, and the minimization process is under-determined, thereby allowing the existence of non-zero global minima. Refining the mesh, the approximation improves up to a maximum precision imposed by the chosen network architecture and the Tensorflow deep learning framework.

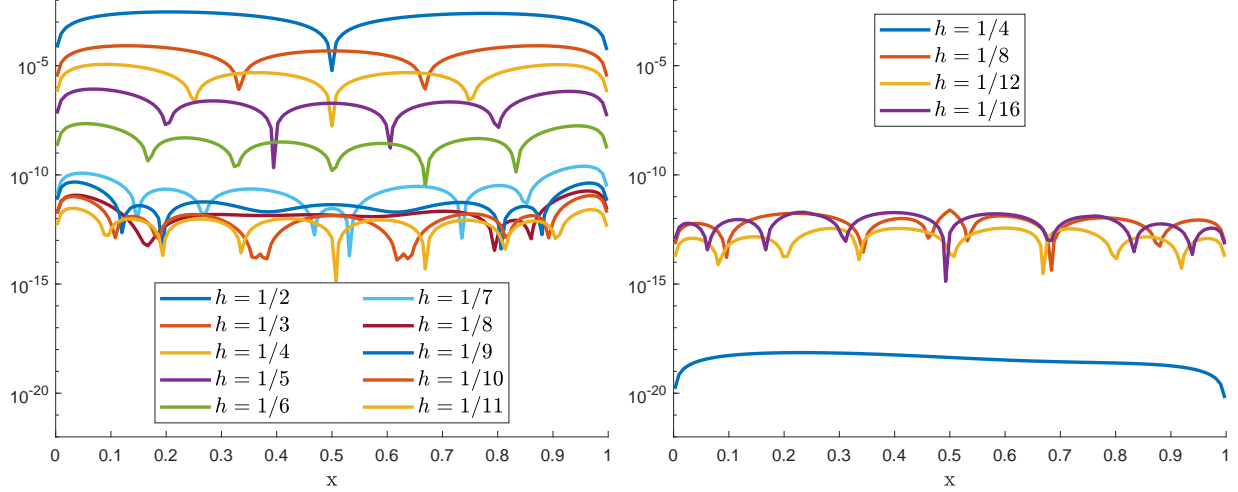


Fig. 9 Numerical solutions of problem (6.4) computed with different meshes, solutions obtained with non-interpolated neural networks (left) and with interpolated neural networks (right). Quadrature rule order $q = 3$. Test functions order $k_{test} = 1$.

Conversely, the plots in the subfigure on the right-hand side of Fig. 9, produced by interpolated networks, clearly indicate that the obtained discrete solutions are numerically zero, irrespective of the meshsize. Note that the case $h = 1/4$ differs from the others since here the interpolation mesh \mathcal{T}_H is formed by just one element. The corresponding function $u_H^{\mathcal{NN}}$ is thus differentiable everywhere and the used gradient-based optimizers are able to minimize the loss function more effectively. We recall that for parameter set P_1 we choose $H = 4h$ to satisfy the inf-sup condition.

These results, although obtained in an overly simple setting, show the potential existence of uncontrolled components in the discrete solutions obtained by non-interpolated neural networks. In more complex scenarios, the presence of spurious modes may be even more pronounced. In practice, as documented in Sects. 6.1 and 6.2, non-interpolated solutions appear to be more accurate than the corresponding solutions obtained by interpolated neural networks; however, a rigorous analysis of neural-network based discretization schemes should also cope with the presence of spurious components, which we have avoided by resorting to an inf-sup condition. We believe that these observations shed new light on the use of deep learning in numerical PDEs.

6.4 Remarks on the convergence rate

Theorem 4.9 indicates that the best possible convergence rate, when the solution is regular enough, is k_{int} . However, as discussed in Remark 4.10, the quotient $\frac{C_h}{c_h}$ is of order $O(h^{-1})$ when test functions are picked from the Lagrange basis associated with a quasi-uniform triangulation, and the weights γ_i are equal to 1. In this case, the term $\left(1 + \frac{C_h}{c_h}\right)$ in (4.33) reduces the predicted convergence by exactly one order.

On the other hand, in Sects. 6.1 and 6.2, we have shown cases where the order of convergence is optimal, together with cases where it is not; in the latter case, the deviation from optimality is precisely by one order. In Remark 4.10, this phenomenon has been related to a different behavior of the loss functions, precisely whether the minimization inequality $R_h(u^{\mathcal{NN}}) \leq R_h(\tilde{w}^{\mathcal{NN}})$, used in the proof of (4.33), may be replaced by the stronger inequality (4.34), where the neural network $\tilde{w}^{\mathcal{NN}}$ realizes a near-best approximation of u according to (4.32).

Hereafter, we document the different behaviors of the loss functions for the problem considered in *Test 1*, with the aim of explaining the decay rates observed in Fig. 2. For the three parameter sets P_1 , P_2 , and P_3 , we plot in Fig. 10 the values of $R_h(u^{\mathcal{NN}})$ and those of $R_h(\tilde{w}^{\mathcal{NN}})$, where $\tilde{w}^{\mathcal{NN}} \in U^{\mathcal{NN}}$ satisfies

$$\tilde{w}^{\mathcal{NN}} = \arg \min_{w \in U^{\mathcal{NN}}} \|u - \mathcal{I}_H Bw\|_{1,\Omega}. \quad (6.5)$$

For the sake of comparison, we also plot the values of $R_h(\tilde{u})$, where \tilde{u} is defined by the representation (2.4) of the exact solution; note that $R_h(\tilde{u})$ should vanish in the absence of quadrature errors, hence, it just measures the effect of quadratures in the loss computation.

Subfigures (10.a) and (10.d) clearly indicate that for parameter sets P_1 and P_2 inequality (4.34) does hold, hence, the quotient $\frac{C_h}{c_h}$ can be removed from the estimate (4.33), thereby predicting the optimal decay rates observed in Fig. 2, left and center plots. Indeed, in these cases, the meshes \mathcal{T}_H and \mathcal{T}_h are such that the minimization problem (3.12) produces a vanishing loss (in exact arithmetics), since the number of interpolation points equals the number of test

functions; in practice, $R_h(u^{\mathcal{NN}})$ reaches values close to machine accuracy. Note that, in subfigure (10.b), fewer points are displayed because numerical issues do not allow us to obtain $R_h(u^{\mathcal{NN}})$ close to machine accuracy for finer meshes.

On the contrary, subfigures (10.c) and (10.d) show that for parameter set P_3 inequality (4.34) does not hold, hence (4.33) correctly predicts the loss of one order of convergence observed in Fig. 2, right plot. In this case, the minimization problem (3.12) is ‘overdetermined’, since when q and $k_{\text{int}} = q + 2 - k_{\text{test}}$ are coprime, the number of test functions has to be larger than the number of interpolation nodes in order to ensure the inf-sup condition; in practice, the minimal losses assume values dictated by the best approximation errors on the corresponding meshes.

Similar considerations can be extended to the other test cases considered in Sects. 6.1 and 6.2.

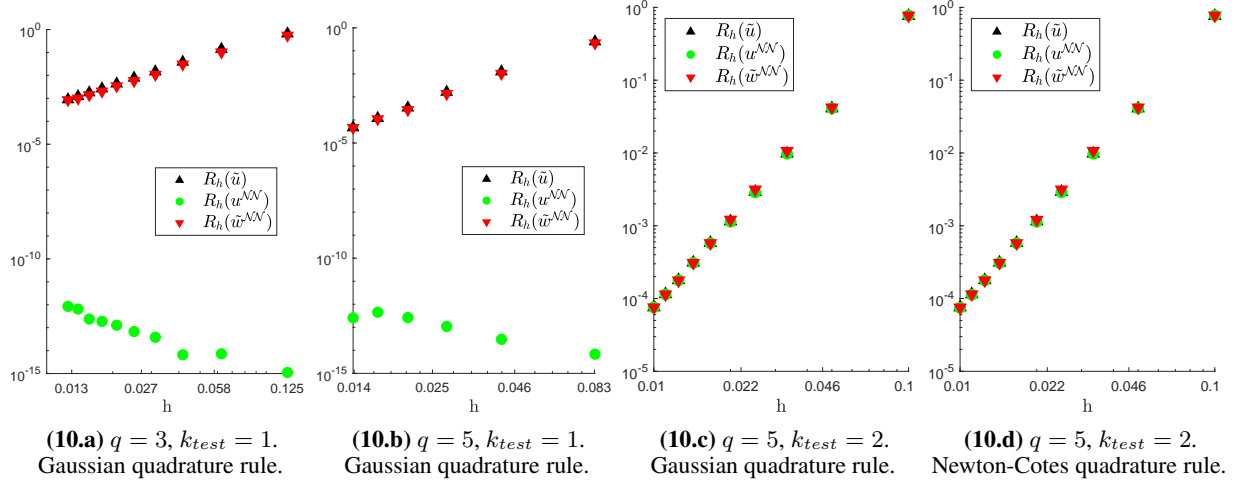


Fig. 10 Residuals computed on \tilde{u} defined in (2.4), on $u^{\mathcal{NN}}$ defined in (4.2) and on $\tilde{w}^{\mathcal{NN}}$ satisfying (6.5).

7 Conclusions

We have investigated VPINN methods for elliptic boundary-value problems, in what concerns the choice of test functions and quadrature rules. The aim was the derivation of rigorous a priori error estimates for some projection of the neural network solution. Test functions were chosen as finite-element nodal Lagrange basis functions of degree k_{test} on a mesh \mathcal{T}_h in the domain; quadrature rules were chosen of either Gaussian or Newton-Cotes type, and of order q . For a fixed neural network architecture with tanh activation function, we studied how the error in the energy norm depends upon the mesh parameter h , for different values of k_{test} and q .

Error control was obtained for the finite-element interpolant of degree $k_{\text{int}} = q + 2 - k_{\text{test}}$ of the neural network on an auxiliary mesh \mathcal{T}_H ; such interpolation enters also in the definition of the residuals which are minimized through the loss function. A key ingredient in the error control is the validity of an inf-sup condition between the spaces of test functions and interpolating functions. Indeed, the neural network solution might be affected by spurious modes due to the under-determined nature of the minimization problem, as we documented for a problem with zero data; the onset of such modes is prevented instead by the adopted interpolation procedure.

Our analysis reveals that the convergence rate in the energy norm is at least of order $q + 1 - k_{\text{test}}$ for sufficiently smooth functions, and it increases to $q + 2 - k_{\text{test}}$ when the value of the loss function obtained by minimization is sufficiently small. The main message stemming from the analysis is that it is convenient to choose test functions of the lowest degree $k_{\text{test}} = 1$ in order to get the highest convergence rate for a fixed quadrature rule. Furthermore, for smooth solution the convergence rate may be arbitrarily increased by increasing the precision of the quadrature rule, although the realization of this theoretical statement is hampered in practice by the finite precision of machine arithmetics.

Interestingly, we experimentally observed that in most cases the error decay rate for the non-interpolated neural network solution replicates the one theoretically predicted for the interpolated network. Actually, in the asymptotic regime the errors of the former network are several orders of magnitude smaller than those of the latter, although some instabilities are observed in the pre-asymptotic regime. We can say that the errors of a non-interpolated VPINN are controlled from above by those of a certified interpolated VPINN.

Several extensions of our analysis are possible. Here we list a few of them.

- i) The functional framework presented in this paper allows an easy derivation of a posteriori error estimates. They are crucial in order to reduce the computational cost of the method, since the most expensive phase is the training one that, at the moment, is performed by a pre-defined number of optimization steps. Relating

the stopping criterion to the value of an a posteriori estimator would increase efficiency. For non-interpolated VPINNs, an a posteriori error estimate is discussed in [24].

- ii) In this paper we adopted the simplest existing neural network architecture, the feed-forward neural network with fixed depth and fixed wideness. It would be interesting to rigorously relate the choice of the architecture parameters (number of layers and weights) to the choice of the PDE discretization parameters h , k_{test} , and q . In a more general perspective, the use of sophisticated network architectures should be explored; we expect that current physics informed neural networks can be significantly improved properly combining physics informed loss function with advanced neural networks architectures. Pioneering works in this direction are, for instance, [21] and [5].
- iii) We focused on linear elliptic problems in order to highlight the essential ingredients of our error analysis; however, we are aware that several mature and efficient numerical technique are available for such problems, and VPINNs can hardly compete with them because of their slow training phase. Interesting benchmarks, in order to understand the strong and weak points of the proposed method, are probably related to nonlinear, parametric or high-dimensional PDEs. In fact, we expect neural network based solvers to efficiently handle nonlinear problems without any additional nonlinear solver or globalization method [23] thanks to their intrinsic nonlinear nature. On the other hand, neural networks are known to be able manage very high-dimensional problems, overcoming the so called curse of dimensionality, therefore we expect them to be able to efficiently solve parametric [5] or high-dimensional PDEs [8, 14].

Acknowledgements. The authors performed this research in the framework of the Italian MIUR Award “Dipartimenti di Eccellenza 2018-2022” granted to the Department of Mathematical Sciences, Politecnico di Torino (CUP: E11G18000350001). The research leading to this paper has also been partially supported by the SmartData@PoliTO center for Big Data and Machine Learning technologies. SB was supported by the Italian MIUR PRIN Project 201744KLJL-004, CC was supported by the Italian MIUR PRIN Project 201752HKH8-003. The authors are members of the Italian INdAM-GNCS research group.

References

- [1] A. G. BAYDIN, B. A. PEARLMUTTER, A. A. RADUL, AND J. M. SISKIND, *Automatic differentiation in machine learning: a survey*, Journal of machine learning research, 18 (2018).
- [2] PH. CIARLET, *The Finite Element Method for Elliptic Problems*, vol. 40 of Classics in Applied Mathematics, Society for Industrial and Applied Mathematics (SIAM), Philadelphia, 2002.
- [3] T. DE RYCK, S. LANTHALER, AND S. MISHRA, *On the approximation of functions by tanh neural networks*, Neural Networks, (2021).
- [4] D. ELBRÄCHTER, D. PEREKRESTENKO, P. GROHS, AND H. BÖLCSKEI, *Deep neural network approximation theory*, IEEE Transactions on Information Theory, 67 (2021), pp. 2581–2623.
- [5] H. GAO, L. SUN, AND J.-X. WANG, *Phygeonet: physics-informed geometry-adaptive convolutional neural networks for solving parameterized steady-state pdes on irregular domain*, Journal of Computational Physics, 428 (2021), p. 110079.
- [6] L. GONON AND C. SCHWAB, *Deep ReLU neural networks overcome the curse of dimensionality for partial integrodifferential equations*, arXiv preprint arXiv:2102.11707, (2021).
- [7] I. GÜHRING, G. KUTYNIOK, AND P. PETERSEN, *Error bounds for approximations with deep ReLU neural networks in $W^{s,p}$ norms*, Analysis and Applications, 18 (2020), pp. 803–859.
- [8] J. HAN, A. JENTZEN, AND E. WEINAN, *Solving high-dimensional partial differential equations using deep learning*, Proceedings of the National Academy of Sciences, 115 (2018), pp. 8505–8510.
- [9] W. JI, W. QIU, Z. SHI, S. PAN, AND S. DENG, *Stiff-pinn: Physics-informed neural network for stiff chemical kinetics*, arXiv preprint arXiv:2011.04520, (2020).
- [10] E. KHARAZMI, Z. ZHANG, AND G. KARNIADAKIS, *VPINNs: Variational Physics-Informed Neural Networks For Solving Partial Differential Equations*, arXiv preprint arXiv:1912.00873, (2019).
- [11] E. KHARAZMI, Z. ZHANG, AND G. E. KARNIADAKIS, *hp-VPINNs: Variational physics-informed neural networks with domain decomposition*, Computer Methods in Applied Mechanics and Engineering, 374 (2021), p. 113547.
- [12] R. KHODAYI-MEHR AND M. ZAVLANOS, *VarNet: Variational neural networks for the solution of partial differential equations*, in Learning for Dynamics and Control, PMLR, 2020, pp. 298–307.
- [13] G. KUTYNIOK, P. PETERSEN, M. RASLAN, AND R. SCHNEIDER, *A theoretical analysis of deep neural networks and parametric PDEs*, Constructive Approximation, (2021), pp. 1–53.

- [14] S. LANTHALET, S. MISHRA, AND G. E. KARNIADAKIS, *Error estimates for deepnets: a deep learning framework in infinite dimensions*, arXiv preprint arXiv:2102.09618v2, (2021).
- [15] S. MISHRA AND R. MOLINARO, *Estimates on the generalization error of physics-informed neural networks for approximating a class of inverse problems for PDEs*, IMA Journal of Numerical Analysis, (2021).
- [16] J. A. NITSCHKE, *Über ein Variationsprinzip zur Lösung Dirichlet-Problemen bei Verwendung von Teilräumen, die keinen Randbedingungen unterworfen sind*, Abh. Math. Sem. Univ., Hamburg, 36 (1971), pp. 9–15.
- [17] J. A. OPSCHOOR, P. C. PETERSEN, AND C. SCHWAB, *Deep ReLU networks and high-order finite element methods*, Analysis and Applications, 18 (2020), pp. 715–770.
- [18] J. A. OPSCHOOR, C. SCHWAB, AND J. ZECH, *Exponential ReLU DNN expression of holomorphic maps in high dimension*, Constructive Approximation, (2021), pp. 1–46.
- [19] M. RAISSI, P. PERDIKARIS, AND G. KARNIADAKIS, *Physics-informed neural networks: A deep learning framework for solving forward and inverse problems involving nonlinear partial differential equations*, Journal of Computational Physics, 378 (2019), pp. 686–707.
- [20] S. REDDI, M. ZAHEER, D. SACHAN, S. KALE, AND S. KUMAR, *Adaptive methods for nonconvex optimization*, in Proceeding of 32nd Conference on Neural Information Processing Systems (NIPS 2018), 2018.
- [21] R. RODRIGUEZ-TORRADO, P. RUIZ, L. CUETO-FELGUEROSO, M. C. GREEN, T. FRIESEN, S. MATRINGE, AND J. TOGELIUS, *Physics-informed attention-based neural network for solving non-linear partial differential equations*, arXiv preprint arXiv:2105.07898, (2021).
- [22] F. SAHLI COSTABAL, Y. YANG, P. PERDIKARIS, D. E. HURTADO, AND E. KUHL, *Physics-informed neural networks for cardiac activation mapping*, Frontiers in Physics, 8 (2020), p. 42.
- [23] Y. SHI, *A globalization procedure for solving nonlinear systems of equations*, Numerical Algorithms, 12 (1996), pp. 273–286.
- [24] Y. SHIN, Z. ZHANG, AND G. E. KARNIADAKIS, *Error estimates of residual minimization using neural networks for linear pdes*, arXiv preprint arXiv:2010.08019, (2020).
- [25] L. N. SMITH, *Cyclical learning rates for training neural networks*, in 2017 IEEE winter conference on applications of computer vision (WACV), IEEE, 2017, pp. 464–472.
- [26] N. SUKUMAR AND A. SRIVASTAVA, *Exact imposition of boundary conditions with distance functions in physics-informed deep neural networks*, arXiv preprint arXiv:2104.08426, (2021).
- [27] A. TARTAKOVSKY, C. MARRERO, P. PERDIKARIS, G. TARTAKOVSKY, AND D. BARAJAS-SOLANO, *Learning parameters and constitutive relationships with physics informed deep neural networks*, arXiv preprint arXiv:1808.03398, (2018).
- [28] C. L. WIGHT AND J. ZHAO, *Solving allen-cahn and cahn-hilliard equations using the adaptive physics informed neural networks*, Communications in Computational Physics, 29 (2021), pp. 930–954.
- [29] S. WRIGHT, J. NOCEDAL, ET AL., *Numerical optimization*, Springer Science, 35 (1999), p. 7.
- [30] Y. YANG AND P. PERDIKARIS, *Adversarial uncertainty quantification in physics-informed neural networks*, Journal of Computational Physics, 394 (2019), pp. 136–152.
- [31] Y. ZANG, G. BAO, X. YE, AND H. ZHOU, *Weak adversarial networks for high-dimensional partial differential equations*, Journal of Computational Physics, (2020), p. 109409.
- [32] E. ZHANG, M. YIN, AND G. E. KARNIADAKIS, *Physics-informed neural networks for nonhomogeneous material identification in elasticity imaging*, arXiv preprint arXiv:2009.04525, (2020).